TOWARDS RANDOM WALKS UNDERLYING NEURONAL SPIKES

Arturo Tozzi
Center for Nonlinear Science, University of North Texas
1155 Union Circle, #311427, Denton, TX 76203-5017, USA, and
tozziarturo@libero.it
Arturo.Tozzi@unt.edu

Alexander Yurkin
Russian Academy of Sciences
Moscow, Puschino, Russia
alvl1yurkin@rambler.ru

James F. Peters
Department of Electrical and Computer Engineering, University of Manitoba
75A Chancellor's Circle, Winnipeg, MB R3T 5V6, Canada and
Mathematics Department, Adiyaman University, Adiyaman, Turkey
james.peters3@umanitoba.ca

The brain, rather than being homogeneous, displays an almost infinite topological genus, because is punctured with a very high number of topological vortexes, i.e., .e., nesting, non-concentric brain signal cycles resulting from inhibitory neurons devoid of excitatory oscillations. Starting from this observation, we show that the occurrence of topological vortexes is constrained by random walks taking place during self-organized brain activity. We introduce a visual model, based on the Pascal's triangle and linear and nonlinear arithmetic octahedrons, that describes three-dimensional random walks of excitatory spike activity propagating throughout the brain tissue. In case of nonlinear 3D paths, the trajectories in brains crossed by spiking oscillations can be depicted as the operation of filling the numbers of the octahedrons in the form of "islands of numbers": this leads to excitatory neuronal assemblies, spaced out by empty area of inhibitory neuronal assemblies. These procedures allow us to describe the topology of a brain of infinite genus, to assess inhibitory neurons in terms of Betti numbers, and to highlight how non-linear random walks cause spike diffusion in neural tissues when tiny groups of excitatory neurons start to fire.

Keywords: arithmetic figures; Pascal's triangle; geometrization of brain; central nervous system; nonlinear.

In this paper, we will tackle the issue of a scarcely observed topological property of the brain. The most successful accounts implicitly assume that the brain is a Riemannian manifold with genus zero (Friston and Ao, 2012; Telley et al., 2019). Genus is a particular topological invariant, generally used for classification of 2D manifolds, linked to the Euler characteristic, which generalizes to higher dimensions. However, the brain displays countless holes, *i.e.*, the transient neuronal "punctures" with inhibitory activity (Hodge et al, 2019). We will term these neurons devoid of excitatory spikes "brain vortexes". This means that the brain is equipped with a countless, or at least very high, number of holes surrounding excitatory spiking neurons. Assuming that the brain is isotropic/homogeneous at very large scales and that the excitatory/inhibitory ratio is constant, the tissue concentration of these holes might be regular. To make a trivial example, we might think to the brain as a sponge equipped with countless, uniformly placed, holes. Therefore, we ask: how are brain vortexes produced during nervous activity, within the geometric dynamics on a 3D manifold of infinite genus? The answer lies in the conserved differentiation programs, together with later-occurring environment-dependent signals, that act on sequential ground states (Telley et al., 2019; Velasco et al., 2019).
What are the topological features, peculiarities and predictable physical consequences of a brain described in terms of a Riemannian manifold with very high, almost infinite, genus? To answer these questions, we introduce a deterministic geometric model that permits visual constructions of linear (without any acceleration) and nonlinear (with the simplest uniformly acceleration) random walks in three-dimensional spaces. Our model is derived from the Pascal's triangle, an array of the binomial coefficients widely used in numerous contexts. Its applications in mathematics extend to algebra, calculus, trigonometry, plane and solid geometry. The two major areas where Pascal's Triangle is used are algebra and probability/combinatorics (Edwards 2013). It is a useful tool in finding, without tedious computations, the number of subsets of r elements that can be formed from a set with n distinct elements (Brothers 2012). In the real world, this leads into the complex topic of graph theory (turning mapping information into structures such as shortest paths, airplane routes and airport control, Dijkstra's algorithm, computer graphics, engineering, search algorithms and data management). In a triangular portion of a grid, the number of shortest grid paths from a given node to the top node of the triangle is the corresponding entry in Pascal's triangle. The pattern produced by an elementary cellular automaton using rule 60 is exactly the Pascal's triangle of binomial coefficients reduced modulo 2. Further, to provide a last

example, Proton Nuclear Magnetic Resonance displays an inherent geometry in which Pascal's triangles has a prominent role (Hore 1983).
In the following, we will show how Pascal's triangle-derived models are able to describe the paths of random walks leading to short- and long-range brain oscillations and to explain the formation of brain vortexes.

GEOMETRIC MODEL OF RANDOM WALKS

Simple and visual geometric models are needed to substantiate the consistency in describing complex phenomena (Klein 1956; Sommerfeld 1973). Here we propose various recursive formulas for calculating the step-shaped Pascal's triangle at various initial conditions, to assess cosmic random walks processes.
Pascal's arithmetic triangle, its analogues, generalizations and possible applications of visual geometric models have been thoroughly carried out (Yurkin, 2013, 2016, 2018; Yurkin et al., 2018). Novel, stepwise form for Pascal's triangle (1D), two-sided (2D) and multidimensional generalizations can be achieved in linear models of random walks (Kolmogorov et al., 1995). Yurkin (1995) proposed an optical laser scheme standing for a nonlinear 1D walk in a system of rays; further, a real laser nonlinear 2D random walk in a system of rays was carried out. Nonlinear and non-Markovian random walks were described by Fedotov and Korabel (2015). Sarkar an Maiti (2017) described a symmetric random walk on a regular tetrahedron, an octahedron and a cube. In the 1D case (along a straight line), a random walk (linear and nonlinear) can occur along two mutually perpendicular directions (right, left) inside an arithmetic triangle (the triangle has two corners on his base and one on his top) (Kolmogorov et al., 1995). In the 2D case, a random walk (linear and nonlinear) can be carried out in four different directions (forward, back, right, left) inside an arithmetic square (the square has four corners) (Yurkin 2019).
In this paper, we aim to assess visual linear and nonlinear 3D models in form of arithmetic octahedrons to describe linear and nonlinear 3D random walks. In the 3D case of a Pascal's triangle, a random walk (linear and nonlinear) can be carried out in six different directions (forward, backward, right, left, up, down) inside an octahedron equipped with six vertices.

Linear random 3D walk in the octahedron. A 3D linear random walk or a walk in a volume can be described using a 3D model in the form of an arithmetic regular octahedron. We achieve the linear binomial coefficients in the computed cell of the octahedron n by summing the numbers from the six cells adjacent to the computed cell.
Figures 1-4 show sequentially, for the first four iterations, images of linear arithmetic octahedrons composed of small cubes. The parts of the **Figures 1-4** termed with (a) show images of the arithmetic octahedrons themselves, while (b) show images of layers of octahedrons composed of small cubes containing numbers. These numbers correspond to the number of walks from the initial cell (initial cube) to the final cell (final cube).

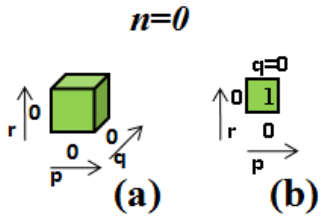

Figure 1. The zero linear arithmetic octahedron (zero iteration $n = 0$) consists of 1 cube.

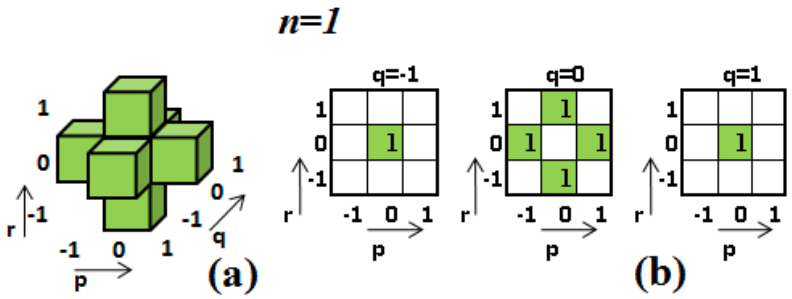

Figure 2. The first linear arithmetic octahedron (the first iteration $n = 1$) consists of 6 cubes.

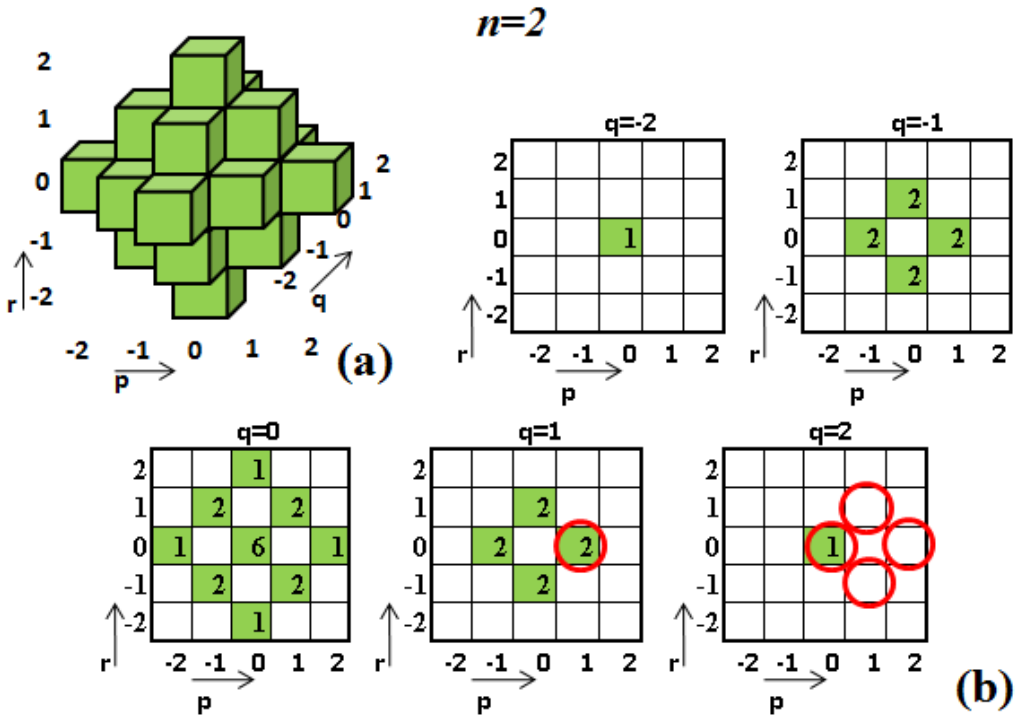

Figure 3. The second linear arithmetic octahedron (second iteration $n = 2$) consists of 19 cubes.

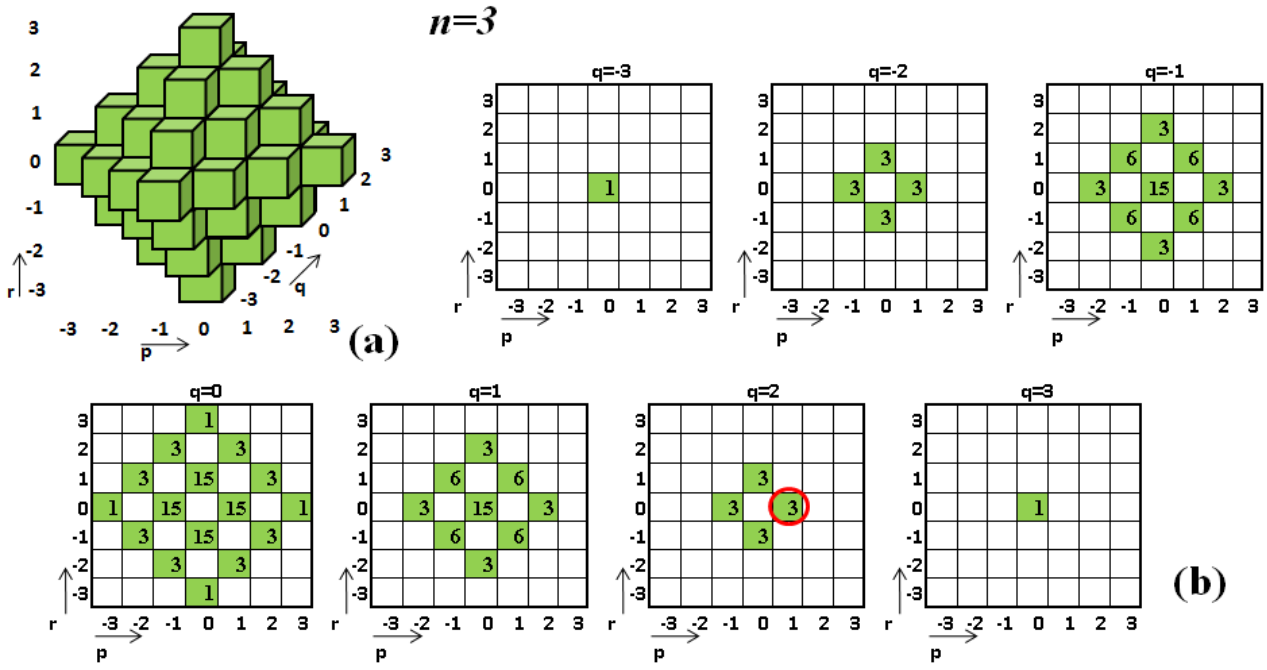

Figure 4. The third linear arithmetic octahedron (the third iteration $n = 3$) consists of 44 cubes.

The sequence of numbers of octahedrons in the example is denoted by $n: = 0, 1, 2, ...$ The total sum of numbers in octahedrons is 6^n. The numbers characterizing the octahedron (which describe the location of the cubes composing the octahedron) are denoted p, q and r:

$$p = 0, \pm1, \pm2, \dots, \pm n; q = 0, \pm1, \pm2, \dots, \pm n: r = 0, \pm1, \pm2, \dots, \pm n. \quad (1)$$

Denote a number located in the n – octahedron as $\binom{n}{p}_{q}^{r}$, then specify the number of the zero octahedron ($n = 0$), or, in other words, the initial conditions:

$$\binom{0}{p}_{q}^{r} = 1 \text{for } p = 0, q = 0, r = 0 \text{ and } \binom{0}{p}_{q}^{r} = 0 \quad (2)$$

for the other values p, q and r.

The numbers in the linear arithmetic octahedron are linear binomial coefficients $\binom{n}{p}_{q}^{r}$. They can be can be calculated using the recursive 3D linear expression:

$$\binom{n}{p}_{q}^{r} = \binom{n-1}{p}_{q-1}^{r} + \binom{n-1}{p}_{q}^{r+1} + \binom{n-1}{p-1}_{q}^{r} + \binom{n-1}{p+1}_{q}^{r} + \binom{n-1}{p}_{q}^{r-1} + \binom{n-1}{p}_{q+1}^{r}. \quad (3)$$

Example 1: $n = 3, p = 1, q = 2, r = 0$.

$$\binom{3}{1}_{2}^{0} = \binom{2}{1}_{1}^{0} + \binom{2}{1}_{2}^{1} + \binom{2}{0}_{2}^{0} + \binom{2}{2}_{2}^{0} + \binom{2}{1}_{2}^{-1} + \binom{2}{1}_{3}^{0} = 3,$$

as

$$\binom{2}{1}_{1}^{0} = 2, \binom{2}{1}_{2}^{1} = 0, \binom{2}{0}_{2}^{0} = 1, \binom{2}{2}_{2}^{0} = 0, \binom{2}{1}_{2}^{-1} = 0, \binom{2}{1}_{3}^{0} = 0.$$

In **Figures 3** and **4**, these numbers are circled in red circle, except for the number $\binom{2}{1}_{3}^{0} = 0$, which goes beyond the square in **Figure 3** in accordance with the expression (13); for this number: $q = 3 > n = 2$.

Figures 2-4 show that the octahedrons are densely filled with green cubes (branching cells). Neighboring empty cells inside octahedrons (white cubes or gaps) will be filled with green cubes at the next iteration. We can say that numbers densely (without spaces) fill the linear arithmetic octahedrons.

Nonlinear random 3D walk in the octahedron. To describe a nonlinear 3D random walk, we calculate nonlinear coefficients using the recursion formula given below and check it in the Figures. A 3D nonlinear random walk or a walk in a volume can also be described, like a linear one, using a 3D model in the form of a nonlinear arithmetic regular octahedron. Nonlinear binomial coefficients in the computed cell of the octahedron $n = 1$ are obtained by summing the numbers of six cells adjacent to the computed cell; nonlinear binomial coefficients in the cell of the octahedron $n = 2$ we get by summing the numbers of six cells located one through the calculated cell; nonlinear binomial coefficients in the cell of the octahedron $n = 3$ we get by summing the numbers of six cells located two through the calculated cell; etc.

Figures 5-8 show sequentially (for the first four iterations) images of the nonlinear arithmetic octahedrons composed of small cubes. **Figures 5-8** termed with (a) show images of the arithmetic octahedrons themselves, while (b) show images of layers of octahedrons composed of cubes containing numbers. These numbers correspond to the number of walks from the initial cell (initial cube) to the final cell (final cube).

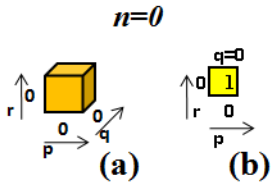

Figure 5. The zero nonlinear arithmetic octahedron (zero iteration $n = 0$) consists of 1 cube.

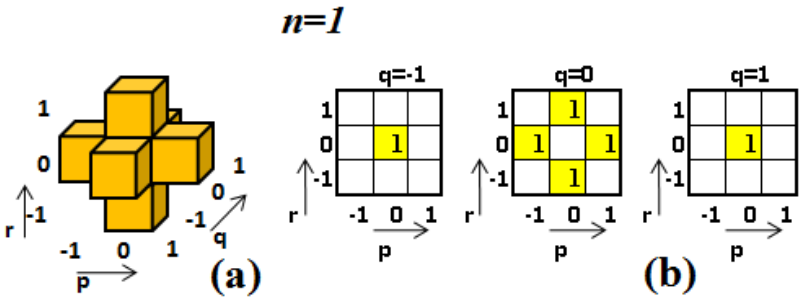

Figure 6. The first nonlinear arithmetic octahedron (the first iteration $n = 1$) consists of 6 cubes.

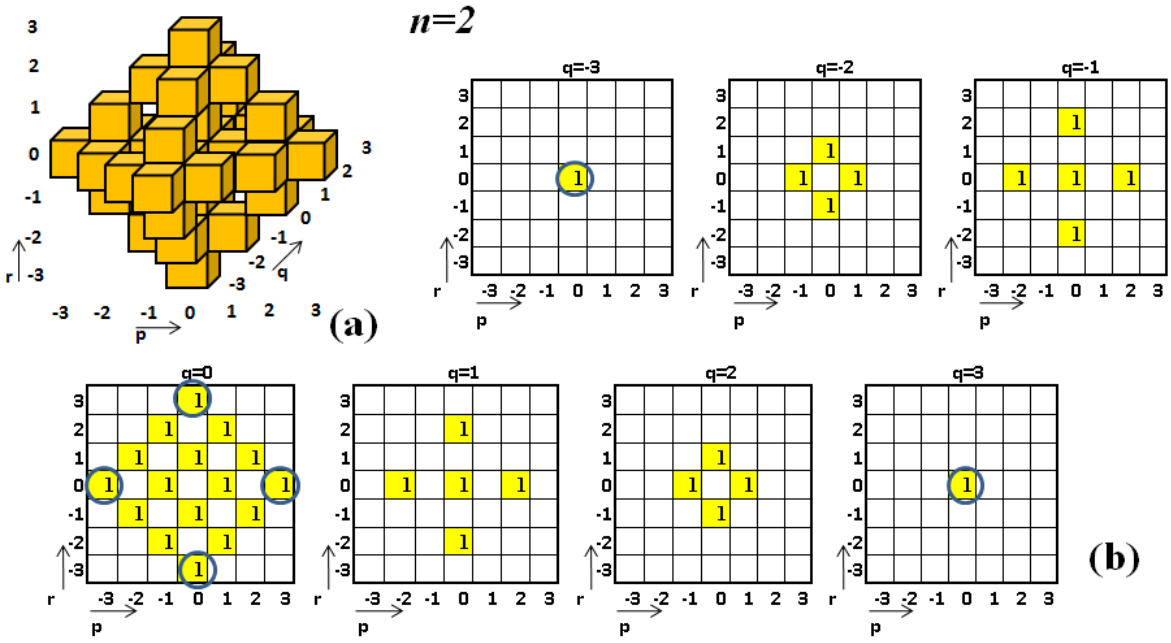

Figure 7. The second nonlinear arithmetic octahedron (the second iteration $n = 2$) consists of 36 cubes. The Figures $q = \pm 1$ clearly show the formation of separate structures of numbers ("islands of numbers").

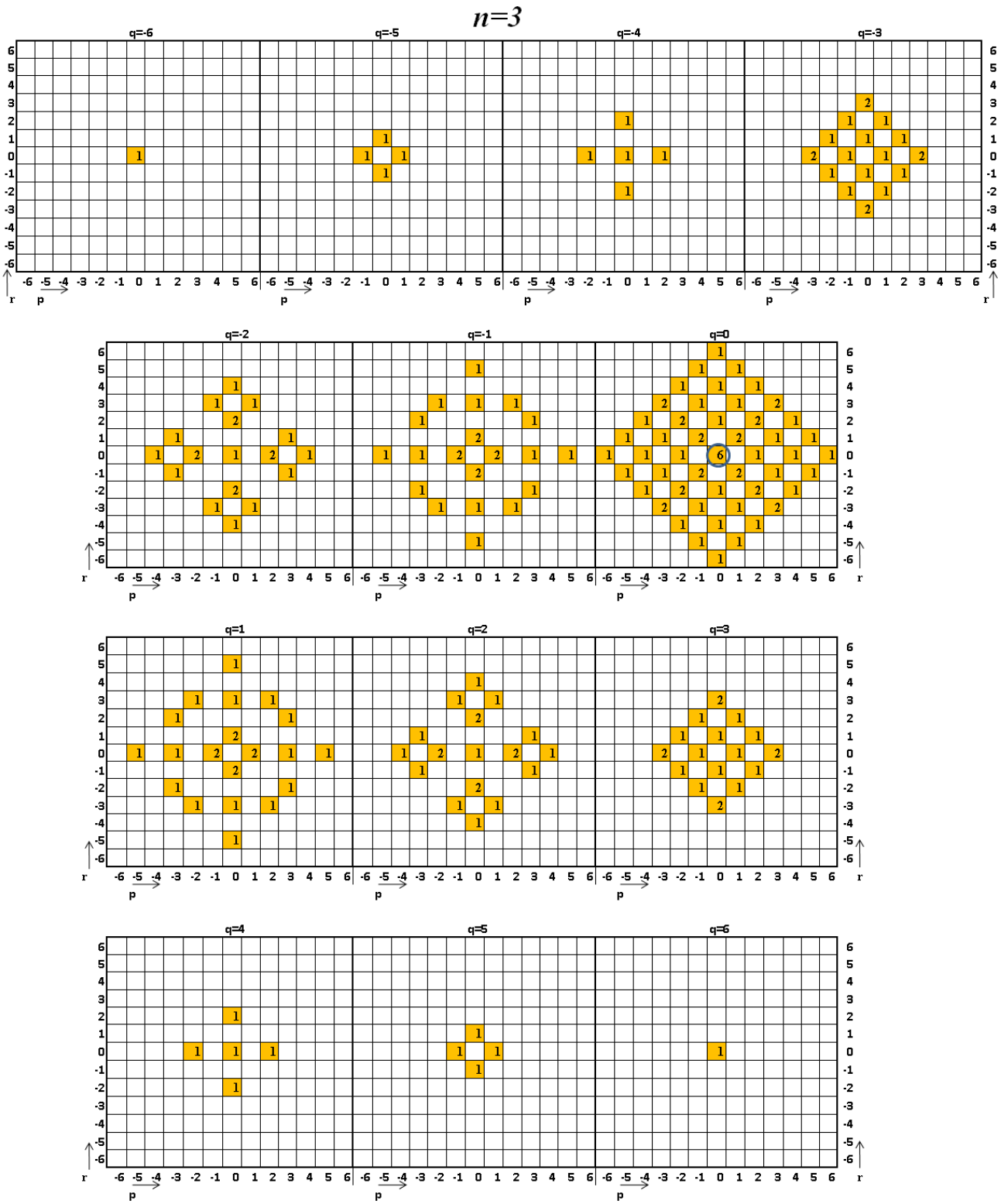

Figure 8. The third nonlinear arithmetic octahedron (the third iteration $n = 3$) consists of 175 cubes. The Figures $q = \pm 1, q = \pm 2, q = \pm 4$ clearly show the formation of separate structures of numbers ("islands of numbers"). The image of the corresponding octahedron is not dispalyed.

The sequence of numbers of octahedrons (rows of numbers in the octahedron) for the 3D case in this example is denoted by n: $n = 0, 1, 2, \ldots$. The total sum of numbers in octahedron is 6^n. The numbers characterizing the nonlinear octahedron (the numbers illustrating the position of the cubes of which the octahedron is composed) are denoted by p, q and r:

$$\left.\begin{array}{c} p = 0, \pm 1, \pm 2, \ldots, \pm n(n+1)/2; \\ q = 0, \pm 1, \pm 2, \ldots, \pm n(n+1)/2; \\ r = 0, \pm 1, \pm 2, \ldots, \pm n(n+1)/2. \end{array}\right\} \quad (4)$$

Denote a number located in the n - octahedron as $\binom{n}{p}{q}{r}$ then specifies the number of the zero octahedron ($n = 0$), or in other words, the initial conditions:

$$\binom{0}{p}{q}{r} = 1 \text{for } p = 0, q = 0, r = 0 \text{ and } \binom{0}{p}{q}{r} = 0 \quad (5)$$

for the other values of p, q and r.

The numbers in the nonlinear arithmetic octahedron are nonlinear binomial coefficients $\binom{n}{p}{q}{r}$, $w\square ic\square$ can be found using the recursive 3D nonlinear expression:

$$\binom{n}{p}{q}{r} = \binom{n-1}{p}{q-n}{r} + \binom{n-1}{p}{q}{r+n} + \binom{n-1}{p-n}{q}{r} + \binom{n-1}{p+n}{q}{r} + \binom{n-1}{p}{q}{r-n} + \binom{n-1}{p}{q+n}{r}. \quad (6)$$

Example 2: $n = 3, p = 0, q = 0, r = 0$.

$$\binom{3}{0}{0}{0} = \binom{2}{0}{-3}{0} + \binom{2}{0}{0}{3} + \binom{2}{-3}{0}{0} + \binom{2}{3}{0}{0} + \binom{2}{0}{0}{-3} + \binom{2}{0}{3}{0} = 6,$$

as

$$\binom{2}{0}{-3}{0} = 1, \binom{2}{0}{0}{3} = 1, \binom{2}{-3}{0}{0} = 1, \binom{2}{3}{0}{0} = 1, \binom{2}{0}{0}{-3} = 1, \binom{2}{0}{3}{0} = 1.$$

In **Figures 7-8**, these numbers are circled in blue.

Figures 6-8 illustrate that the octahedrons are not tightly filled with yellow cubes (branching cells). Some empty cells inside the octahedrons (white cubes or gaps) will be filled with yellow cubes at the next iteration, and some empty cells will be filled after several iterations, and some empty cells will be filled after many iterations, and so on. Our numerical calculations show that for big n numbers the relative quantity of the empty cells or gaps (relative to the general quantity of cells in nonlinear octahedron) decreases with n increasing.

BRAIN RANDOM WALKS COME INTO PLAY

The results achieved in the previous paragraphs allow the classification of different types of random walks in the form of the following table:

	Linear random walk (one unit steps, perpendicular each others)	**Nonlinear random walk** (first one unit steps, second two units steps, third three unit steps, ets., perpendicular each others)
3D case	• Steps of constant length along six perpendicular directions in octahedron. • Gaps and "islands of numbers" are absent in a linear arithmetic octahedron.	• Steps of increasing length along six perpendicular directions in octahedron. • Gaps and "islands of numbers" appear and disappear in different areas in a nonlinear arithmetic octahedron after several or many iterations. The relative quantity of the empty cells or gaps decreases with n increasing.

Self-organizing brain oscillations. The above-described Pascal's triangle-framed geometric linear/nonlinear constructions and recursive formulas may find application to understand the activity of neuronal oscillations starting from 3D random walks. Indeed, the brain is a complex, non-linear system operating at the edge of chaos, where inter-dependent modules display spontaneous, self-organized emergent properties (Tognoli and Kelso, 2013; Fraiman and Chialvo, 2012; Xu and Wang, 2014; Tozzi et al., 2016). The brain manifold is equipped with phase spaces where particle movements take place, with trajectories displaying different paths (Wang et al., 2017). The occurrence of spontaneous, genetic-driven oscillations during human brain development has been widely studied, also in syntetic models. For example, it is well-known that spontaneous cortical electric fluctuations are already present by the 34th week of gestation (Krueger et. al., 2014) and are more frequently observed in immature synapses (Kavalali et al. 2011). Further, the vertebrate spinal cord and brainstem are equipped with central pattern generator circuits able to generate meaningful functional output also in absence of sensory inputs. Neocortical circuits can be regarded as plastic types of such pattern generator circuits: indeed, they not just display rich spontaneous dynamics engaged by sensory inputs, but are also able to generate output independent of external stimuli (Yuste et.al., 2005). Trujillo et al. (2019) highlighted how structural and transcriptional changes in network activity spontaneously follow fixed genetic programming in human neocortical organoid models. These organoids exhibited phase-amplitude coupling during network-synchronous events that are similar to human preterm neonatal EEG features; furthermore, they exhibited spontaneous increases in electrical activity dependent on glutamatergic and GABAergic signaling, over the span of several months during maturation. The transcriptional or epigenetic heterogeneity related to early biases in cell fate choices can be externally induced or stochastic in nature (Soldatov et al., 2019). In terms of the Pascal's triangle model, the filled cells stand for single excitatory neurons which number is progressively expanding in the brain, while the empty cells progressively produced inside the octahedrons stand for inhibitory neurons, which number progressively increases (**Figure 9**). At the next iterations, the empty cells will be progressively filled with yellow cubes: this means that areas of inhibition and excitation continuosly appear and disappear, when further iterations take place during the expansion of the spike oscillation.

Bifurcations and excitability in brain. In touch with the framework theorized by Pascal's triangle iterations, the steps progression of nervous spikes has been already described in the brain. To provide an example, in touch with our Pascal's triangle framework, it is well-known that neural crest cells differentiate through a series of stereotypical lineage-restriction binary decisions that involve coexpression/competition of genes driving alternative fate programs (Soldatov et al., 2019). Multipotent neural crest cells decide among the multiple downstream available competing fates and step through a progression of fate bifurcations during migration that can be formalized as a series of sequential binary decisions. Wang et al. (2019) investigated the effects of spontaneous electromagnetic induction on organization processes of self-organized neuronal networks. They found that spontaneous electromagnetic induction slows down self-organization processes by decreasing neuronal excitability, resulting in a more homogeneous directed-weighted network structure with lower causal relationship and less modularity. Furthermore, spontaneous electromagnetic induction is able to reconfigure synaptic connections to optimize economical connectivity patterns (Wang et al., 2019). These data highlight the critical role of spontaneous electromagnetic induction in the formation of an economical self-organized neuronal network. Velasco et al. (2019) demonstrated in organoid models of the dorsal forebrain that reproducible and highly constrained development of the cellular diversity of the central nervous system does not require the embryonal growing environment. Whereas acquisition of ground states by daughter neurons is largely environment-independent, epigenetically regulated cell-extrinsic processes come into play at later stages to sculpt final identity, as demonstrated by the progressive emergence of input-dependent transcriptional programs (Telley et al., 2019).

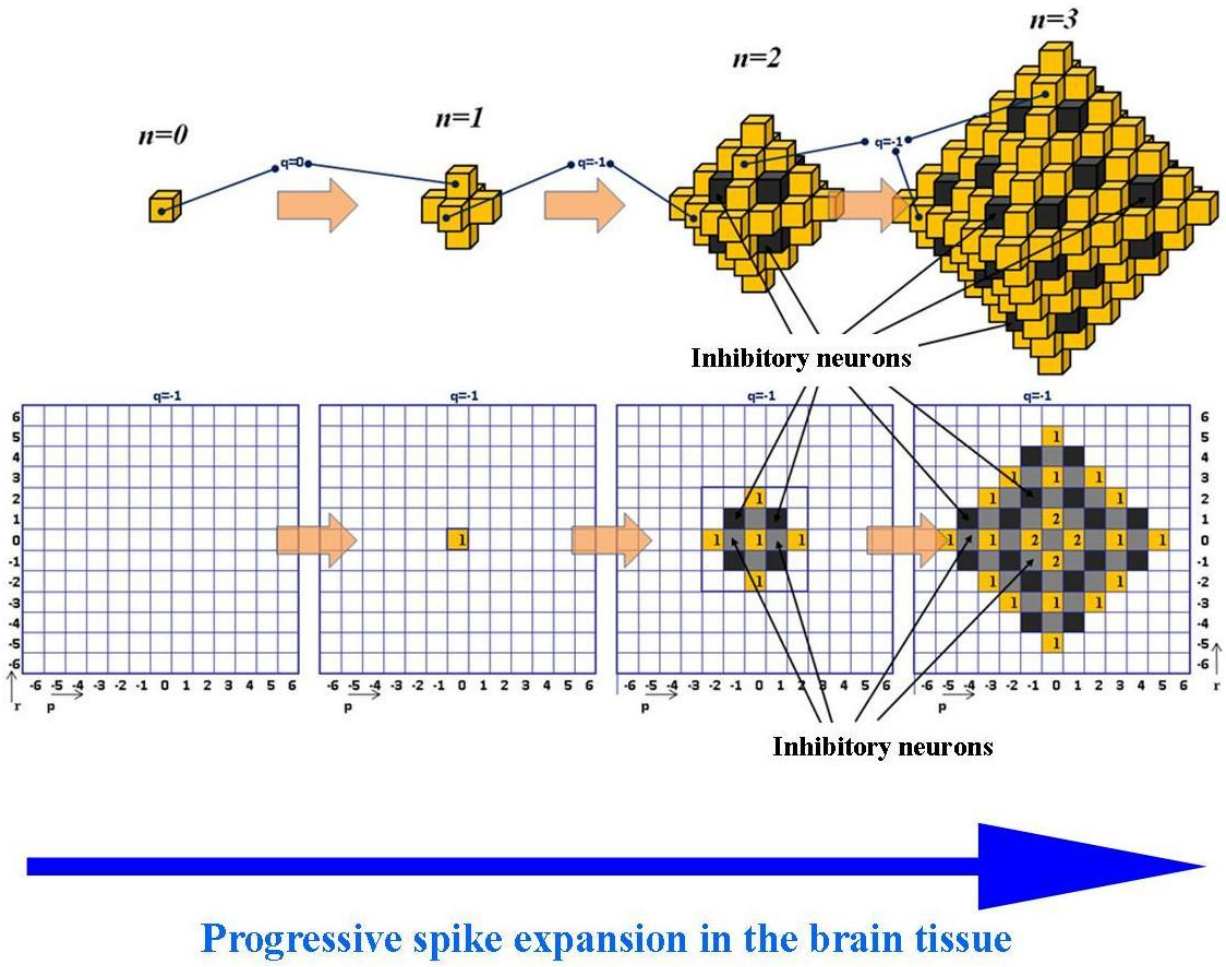

Figure 9. Oscillation expansion and excitatory/inhibitory occurrence in terms of random walks taking place inside a 3D lattice. In our octahedron model, inhibitory neurons look like gaps.

Vortex cycles in brain spikes. A punctured manifold is analogous to a physical/biological space with holes. This means that we need to work on a manifold that is Riemannian. Briefly, a manifold is a topological space that is locally Euclidean (i.e., around every point, there is a neighborhood that is topologically the same as the open unit ball in R^n). A Riemann surface is a surface-like configuration that covers the complex plane with several, and in general infinitely many, "sheets". A sample Riemannian surface is shown in **Figure 10**. It is easy to notice that the center of the surface is punctured with a hole, which stands, in our framework, for a rupture of neuronal excitability due to inhibitory components. Inhibitory neurons can be modelled as vortex cycles (Peters, 2018; Peters, 2020) with induced order proximity of spiraling hole vortexes (Ahmad and Peters, 2019). The rim of this brain vortex cycle represents the edge of an inhibitory neuronal assembly. The inner cycles for a vortex reaching inward represent excitatory brain pull. Therefore, the brain can be depited as nesting, non-concentric vortex cycles embedded in a punctured Riemann surface (Weyl, 1955).

In this context, a novel formulation of the Borsuk Ulam theorem (BUT) might be of great help: the Vortex-BUT, which works on a manifold with holes. There are three forms of vortexBUT:

- physical geometry vortex BUT (pevBUT): each pair of antipodal vortex hypersphere surface points $S^{n-1}(R^n)$ maps to the Euclidean space R^n.
- region-based vortex BUT (revBUT): each pair of antipodal vortex hypersphere surface regions in $2^{S^{n-1}}$ (2^{R^n}) region points map to the Euclidean space 2^{R^n} (Peters, 2016).
- descriptive vortex BUT (phivBUT): each pair of anitipodal vortex surface points OR regions maps to R^k, k >= 1.

Each glial structure is an example of a massive vortex cycle. A punctured physical surface is a surface populated by vortices: this allows us to start viewing punctured brain surfaces using vortexBUT. The one very different thing about the new form of BUT is that we replace the Borsuk-Ulam use of S^n with V^n, a vortex in n-dimensional space. Then the simplest form of vortexBUT is defined by a continuous function

$f: V^n \rightarrow R^n$

so that $f(x) = f(-x)$ for antipodal points x,-x on V^n.

Several variants of BUT have been provided in the very last years to assess brain functions (Tozzi et al., 2017). Why do we need another BUT variant? The answer is straightforward, if we consider that single neurons may have an impact on surround firing statistics and even on simple behaviors. Exploiting the advantages of a simple cortex, Hemberger et al. (2019) examined the influence of single pyramidal neurons on their surrounding cortical circuits. Brief activation of single neurons triggered reliable sequences of firing in tens of other excitatory/inhibitory cortical neurons, reflecting cascading activity through local networks. The evoked pyramidal patterns extended over hundreds of micrometers from their source over up to 200 ms. In touch with a vortexBUT account of the brain, simultaneous activation of pyramidal cell "pairs" (i.e., neuronal activities with matching description as dicatated by BUT) stand for balanced control of population activity, preventing paroxysmal amplification. Single cortical pyramidal neurons can generate rapidly evolving and non-random firing sequences, in touch once again with our Pascal triangle's model (Hemberger et al., 2019).

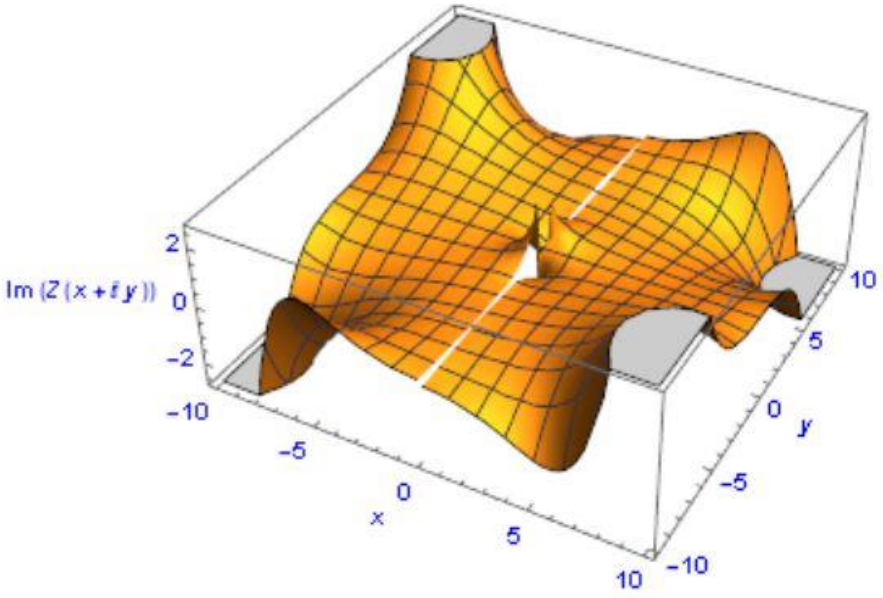

Figure 10. A Riemannian surface with the center of the surface punctured with a hole.

CONCLUSIONS

Our account of deterministic models and visual constructions of linear and nonlinear 3D random walks through arithmetic figures display various interesting geometric properties. In 3D spaces encompassing linear random walks, the achieved arithmetic octahedron is densely filled with numbers (**Figures 2–4**). In 3D spaces encompassing nonlinear random walks, the achieved arithmetic octahedron is not completely filled with numbers, i.e., it contains gaps. Indeed, some neighboring regions inside the nonlinear octahedron remain empty until either the very next iteration, or during several or many iterations. Gaps and "islands of numbers" or separate structures of numbers consistently appear and disappear after several or many iterations in the nonlinear 3D case (**Figures 6–8**). For high n numbers, the relative quantity of the empty cells or gaps (relative to the general quantity of cells in nonlinear octahedron) decreases with n increasing. In sum, for nonlinear 3D cases, we can speak of filling the numbers of the arithmetic octahedron in the form of "islands of numbers" or separate structures of numbers: this leads us into the realm of a nonlinear brain

punctured with inhibitory components that break the topological order of the neuronal tissue and propagating oscillations. The fact that physical constraints, such as the ones described by Pascal's triangle permutations, limit the range of brain activity has been largely recognized in brain growth too. In an intriguing paper, Tripathy et al. (2018) reported that Mast1, espressed just in postmitotic neuronal dendritic and axonal compartments, is associated with the microtubule cytoskeleton in a MAP-dependent manner. Mice with Mast1 microdeletions display peculiar macroscopic features, such as enlarged corpus callosum and smaller cerebellum, in absence of megalencephaly. These opposite findings (abnormal increase vs abnormal reduction) let us to hypothesize that the macroscopic growth of the brain tissue is regulated by physical constraints: keeping invariant the brain size (i.e., in absence of megaloencephaly), the central nervous tissue of animals harboring Mast1 microdeletions undergoes a general rearrangement. In physical/mathematical terms, a three-dimensional lattice (standing for the whole brain mass) harbors vectors and tensors which product (including excitatory and inhibitory neurons) must be held constant. When lattice perturbations occurs(as in the case of cytoskeleton's genetic Mast1 alterations), one of the tensors modifies. In order to keep invariant the tensor product, another tensor need to vary: in simpler words, the fact that more axons cross the midline in Mast1 Leu278 del mice means that the size of other structures (in this case, the cerebellum) must decrease. In touch with this observation, Tripathy et al. (2018) report that, in animals harboring Mast1 microdeletions, the PI3K/AKT3/mTOR pathway is unperturbed, whereas Mast2 and Mast3 levels are diminished, indicative of a dominant-negative mode of action.

In our framework, the combinatorial properties of the Pascal's triangle are correlated with the mathermatical operations that lead to brain spikes, through iterated random walk patterns. The occurrence of inhibitory cells in terms of "hollows" in the very structure of the brain tissue permits us to consider the topological features of a high-genus manifold, compared with genus-zero manifolds. What does the occurrence of a neural manifold of very high genus physically mean? There are, actually, many ways to generalize the notion of genus to higher dimensions, e.g., Heegaard genus in algebraic topology, arithmetic and geometric genus in algebraic geometry (Almgren and Thurston, 1977). Feldman et al. (1996) tackled the issue of the topological properties of infinite genus Riemann surfaces. They introduced a class of infinite genus Riemann surfaces, specified by means of a number of geometric axioms, to which the classical theory of compact Riemann surfaces up to and, including the Torelli Theorem, extends. The axioms are flexible enough to encompass many interesting examples, such as the heat curve and a connection to the periodic Kadomcev-Petviashvilli equation. Apart from the mentioned accounts, our results suggest the feasibility of another intriguing operational approach, which allows us to generalize the notion of genus to higher dimensions through another powerful weapon: the Betti number. The brain might stand for a manifold equipped with a Betti number corresponding to the number of inhibitory neurons. Betti numbers are topological objects proved to be invariants by Poincaré, and used to extend the polyhedral formula to higher dimensional spaces. Informally, the *k*th Betti number refers to the number of path-connected edges (Kaczynski et al., 2004) embedded in surface holes. For a brain tissue with n vortex cycles and k edges attached between each of the cycles, the Betti number = $n + k$ (Manschot et al., 2012). The brain is a dynamical system where the genus changes continuously, because inhibitory cells' activity may vary. If the brain displays a very high genus, the population of excitatory neurons cannot incresase beyond a given threshold, because, in topological terms, the potential squeezing leaves always holes that cannot be reduced to a single point. The occurrence of high genus might help to elucidate experimental data. Our numerical calculations show that, for big n numbers, the relative quantity of the empty cells or gaps (relative to the general quantity of cells in nonlinear octahedron) decreases with n increasing, until a threshold is reached. Our model provides another way to generate inhibitory activity: the progressive iterations of random walks in an expanding excitatory neural brain lead to the production of hollows, standing for places which can be filled by inhibitory neurons. Therefore, inhibitory structures might appear when starting from nonlinear excitatory random walks occurring in the nervous structures.

Experimental data achieved from available neurotechniques suggest that our brain oscillations are strongly isotropic and homogeneous at macroscales of observation, because a constant excitatory/inhibitory (E/I) ratio between the total amount of excitatory and inhibitory stimulation occurs both in vitro and in vivo (Haider, 2006; de Arcangelis 2010). Is it feasible to correlate our mathematical Pascal's triangle approach with the detected isotropy and homogeneity of E7I ratio? Here the concept of hyperuniformity comes into play, i.e., the anomalous suppression of density fluctuations on large length scales occurring in amorphous cellular structures of ordered and disordered materials (Klatt et al., 2019). The evolution of a given set of initial points takes place when, through Lloyd iterations, each point is replaced by the centre mass of its Voronoi cell. This corresponds to a gradient descent algorithm which allows a progressive, general convergence to a random minimum in the potential energy surface. Klatt et al. (2019) report that systems equipped with different initial configurations (such as, e.g., either hyperfluctuating, or anisotropic, or relatively homogeneous pointsets), converge towards the same high degree of uniformity after a relatively small number of Lloyd iterations (about 10^5). This means that, in the brain's adult stadium, independent of the initial conditions, cell volumes become uniform and the dimensionless total energy converges towards values comparable to the optimal deep local energy minima of the lattice. Therefore, we are allowed to describe brain oscillation expansion in terms of Lloyd iterations, where the initial seeds stand for initial point sets (one or few excited neurons), progressively converted to point sets with a centroidal Voronoi diagram. In other words, the tiny perturbations in the brain oscillations which seed the later formation of excitatory macro-structures might stand for the starting points of the subsequent processes described by Klatt et al. (2019) in terms of

Voronoi cells and described by us in terms of Pascal's triangle models. This would permit us observers to achieve, starting from countless different possible conformations of the brain spikes, the currenlty detected isotropic and homogeneous macrostructure of the E/I ratio in the brain. Indeed, after just 10^5 iterations, every possible initial system must converge towards an hyperuniform state, in which observers perceive the degree of uniformity as very high.

REFERENCES

1) Ahmad MZ, Peters JF. 2019. Proximity induced by order relations. arXiv, 1903.05532v2, 1-22.
2) Askar'yan G, Yurkin A. 1989. New developments in optoacoustics. Sov. Phys. Usp. 32 (4):349 – 356.
3) Almgren FJ Jr, Thurston WP. 1977. Examples of Unknotted Curves Which Bound Only Surfaces of High Genus Within Their Convex Hulls. Annals of Mathematics. Second Series, Vol. 105(3):527-538. DOI: 10.2307/1970922
4) Bañados E, Venemans BP, Mazzucchelli C, Farina EP, Walter F, et al. 2018. An 800-million-solar-mass black hole in a significantly neutral Universe at a redshift of 7.5. Nature, 553, 473–476.
5) Brothers HJ. 2012. Finding e in Pascal's triangle. Mathematics Magazine, 85: 51. doi:10.4169/math.mag.85.1.51
6) de Arcangelis L, Herrmann HJ. 2010.Learning as a phenomenon occurring in a critical state. PNAS 107: 3977-3981.
7) Edwards AWF. 2013. The arithmetical triangle. In Wilson, Robin; Watkins, John J., Combinatorics: Ancient and Modern, Oxford University Press, pp. 166–180.
8) Fedotov S, Korabel N. 2015. Nonlinear and non-Markovian random walk: self-organized anomaly. arXiv:1505.02625v1.
9) Feldman J, Knörrer H, Trubowitz E. 1996. Infinite Genus Riemann Surfaces, Toronto 1995.in Canadian Mathematical Society/ Société mathématique du Canada 1945-1995. Volume/Tome 3. Edited by James B. Carrell and Ram Murty, Canadian Mathematical Society, Ottawa (1996) 91-112.
10) Fraiman D, Chialvo DR. 2012. What kind of noise is brain noise: Anomalous scaling behavior of the resting brain activity fluctuations. Frontiers in Physiology, 3 JUL(July), 1–11. http://doi.org/10.3389/fphys.2012.00307
11) Friston K, Ao P. 2012. Free energy, value, and attractors. Comput Math Methods Med. 2012:937860. doi: 10.1155/2012/937860.
12) Haider B, Duque A, Hasenstaub AR, McCormick DA. 2006. Neocortical network activity in vivo is generated through a dynamic balance of excitation and inhibition. J Neurosci. 26(17):4535-45.Hemberger M, Shein-Idelson M, Pammer L, Laurent G. Reliable Sequential Activation of Neural Assemblies by Single Pyramidal Cells in a Three-Layered Cortex. Neuron. OI:https://doi.org/10.1016/j.neuron.2019.07.017.
13) Hodge RD, Bakken TE, Miller JA, Smith KA, Barkan ER, et al. 2019. Conserved cell types with divergent features in human versus mouse cortex. Nature;573(7772):61-68. doi: 10.1038/s41586-019-1506-7.
14) Hore PJ. 1983. Solvent suppression in Fourier transform nuclear magnetic resonance. Journal of Magnetic Resonance, 55 (2): 283–300. doi:10.1016/0022-2364(83)90240-8.
15) Hosokawa T, Yorke HW, Inayoshi K, Omukai K., Yoshida N. 2013. Formation of primordial supermassive stars by rapid mass accretion. Astrophys J 778, 178.
16) Kaczynski, T., Mischaikov, K., Mrozek, M. 2004. Computational Homology. Springer-Verlag, NY, ISBN 0-387-40853-3.
17) Kavalali ET, Chung C, Khvotchev M, Leitz J, Nosyreva E, Raingo J, Ramirez DM. Spontaneous neurotransmission: an independent pathway for neuronal signaling? Physiology (Bethesda). 2011 Feb;26(1):45-53. doi: 10.1152/physiol.00040.2010.
18) Klatt MA, Lovrić J, Chen D, Kapfer SC, Schaller FM, et al. 2019. Universal hidden order in amorphous cellular geometries. Nature Communications, 10:811.
19) Klein F. *1956*. About so-called non-Euclidean geometry. About the geometry bases. Collection of classical works on Lobachevsky's geometry and development of its ideas. Moscow: Gosizdat.
20) Kolmogorov A, Zhurbenko I, Prokhorov A. 1995. Introduction to the theory of probability. Moscow: Nauka.
21) Krueger C, Garvan C. 2014. Emergence and retention of learning in early fetal development. Infant Behav Dev, 37(2):162-73. doi: 10.1016/j.infbeh.2013.12.007.
22) Manschot, J., Pioline, B., Sen, A. 2012. From black holes to quivers. High Energy Physics doi:10.1007/JHEP11(2012)023.
23) Xu X, Wang R. 2014. Neurodynamics of up and down transitions in a single neuron.CognNeurodyn. 8(6):509-15. doi: 10.1007/s11571-014-9298-9.
24) Peters JF. 2016. Computational Proximity. Excursions in the Topology of Digital Images. Springer Int. Pub., ISBN 978-3-379-30260-7, Zbl1382-68008.

25) Peters JF. 2018. Proximal vortex cycles and vortex nerve structures. Non-concentric, nesting, possibly overlapping homology cell complexes. Journal of Mathematical Sciences and Modelling 1, no. 2, 80-85. ISSN 2636-8692.
26) Peters JF. 2020. Computational Geometry, Topology and Physics. Shape Complexes, Optical Vortex Nerves and Proximities in Digital Images. Springer Int. Pub., ISBN 979-3-030-23191-1, Zbl 07098311.
27) Sarkar J, Maiti SI. 2017. Symmetric Random Walks on Regular Tetrahedra, Octahedra, and Hexahedra. Calcutta Statistical Association Bulletin (2017) 69(1) 110–128.
28) Soldatov R, Kaucka M, Kastriti ME, Petersen J, Chontorotzea T, et al. 2019. Spatiotemporal structure of cell fate decisions in murine neural crest. Science, 364(6444). pii: eaas9536. doi: 10.1126/science.aas9536.
29) Sommerfeld A. 1973. Cognition Ways in Physics. Collection of papers, p. 157. Editor: Smorodinsky J. Moscow: Nauka. (Klein, Riemann und die mathematische Physik. Naturwiss (1919), 7.
30) Telley L, Agirman G, Prados J, Amberg N, Fièvre S, et al. 2019. Temporal patterning of apical progenitors and their daughter neurons in the developing neocortex. Science.;364(6440). pii: eaav2522. doi: 10.1126/science.aav2522.
31) Tognoli E, Kelso JS. 2013. On the Brain's Dynamical Complexity: Coupling and Causal Influences Across Spatiotemporal Scales. Advances in Cognitive Neurodynamics (III), (Iii), 259–265. http://doi.org/10.1007/978-94-007-4792-0
32) Tozzi A, Zare M, Benasich AA. 2016. New Perspectives on Spontaneous Brain Activity: Dynamic Networks and Energy Matter. Front Hum Neurosci. 10:247. doi: 10.3389/fnhum.2016.00247.
33) Tozzi A, Peters JF, Fingelkurts AA, Fingelkurts AA, Marijuán PC. 2017. Topodynamics of metastable brains. Physics of Life Reviews, 21, 1-20. http://dx.doi.org/10.1016/j.plrev.2017.03.001.
34) Tripathy R, Leca I, van Dijk T, Weiss J, van Bon BW, et al. 2018. Mutations in MAST1 Cause Mega-Corpus-Callosum Syndrome with Cerebellar Hypoplasia and Cortical Malformations. Neuron, 100(6):1354-1368. DOI:https://doi.org/10.1016/j.neuron.2018.10.044.
35) Trujillo CA , Gao R, Negraes PD, Yeo GW, Voytek B, Muotri AR. 2019. Complex Oscillatory Waves Emerging from Cortical Organoids Model Early Human Brain Network Development. Cell Stem Cell, 25 (4):558-569.E7. DOI:https://doi.org/10.1016/j.stem.2019.08.002
36) Velasco S, Kedaigle AJ, Simmons SK, Nash A, Rocha M, et al. Individual brain organoids reproducibly form cell diversity of the human cerebral cortex. Nature, 570, pages523–527.
37) Venemans BP, Walter F, Decarli R, Bañados E, Carilli C, et al. 2017. Copious Amounts of Dust and Gas in a z = 7.5 Quasar Host Galaxy. The Astrophysical Journal Letters, 851 (1).
38) Veneziano G. 1998. A Simple/Short Introduction to Pre-Big-Bang Physics/Cosmology. arXiv:hep-th/9802057v2
39) Yurkin A. 1995. System of rays in lasers and a new feasibility of light coherence control. (1995) Optics Communications, v.114, p. 393.
40) Yurkin A. 2013. New binomial and new view on light theory. About one new universal descriptive geometric model. (2013) Lambert Academic Publishing, ISBN 978-3-659-38404-2.
41) Yurkin A. 2016. On descriptive geometrical interpretation of the principle of Pauli, elements of the table of Mendeleyev and the Newtonian laminar current of liquid. (2016) Progress in physics, 12: 149-169.
42) Yurkin A. 2018. And where are fluctuations in quantum-mechanical wave function? Advances in Theoretical & Computational Physics, v. 1. Issue 1.1 -7.
43) Yurkin A, Tozzi A, Peters JF, Marijuán P. 2017. Quantifying Energetic Dynamics in Physical and Biological Systems Through a Simple Geometric Tool and Geodetic Curves. Progress in Biophysics and Molecular Biology 131: 153-161.
44) Yurkin A, Peters JF, Tozzi A. 2018. A novel belt model of the atom, compatible with quantum dynamics. Journal of Scientific and Engineering Research 5(7):413-419. www.jsaer.com.
45) A Yurkin. 2019. Computing Stiks against Random Walk (2019) Advances in Theoretical & Computational Physics, v. 2. Issue 1.1 -6.
46) Yuste R, Jason N. MacLean, Jeffrey Smith & Anders Lansner. The cortex as a central pattern generator. Nature Reviews Neuroscience 6, 477-483 (June 2005) | doi:10.1038/nrn1686.
47) Wang Y, Wang R, Zhu Y. 2017. Optimal path-finding through mental exploration based on neural energy field gradients. CognNeurodyn. 11(1):99-111. doi: 10.1007/s11571-016-9412-2.
48) Wang R, Fan Y, Wu Y. 2019. Spontaneous electromagnetic induction promotes the formation of economical neuronal network structure via self-organization process. Sci Rep; 9(1):9698. doi: 10.1038/s41598-019-46104-z.
49) Weyl H. 1955. The Concept of a Riemann Surface, trans. By G.R. MacLane, Dover Pub. Inc., NY, 191 pp.
50) Wise JH, Regan JA, O'Shea BW, Norman ML, Downes TP, Xu H. 2019. Formation of massive black holes in rapidly growing pre-galactic gas clouds. Nature, 566, 85–88.